Multi-century impacts of ice sheet retreat on sea level and ocean tides in Hudson Bay

Hayden, Anna-Mireille; Gomez, Natalya; Wilmes, Sophie-Berenice; Green, Mattias

Journal of Geophysical Research: Oceans

DOI:
https://doi.org/10.1029/2019JC015104

Published: 01/11/2020

Peer reviewed version

Multi-century impacts of ice sheet retreat on sea level and ocean tides in Hudson Bay

Authors: A.-M. Hayden[1*], S.-B. Wilmes[2], N. Gomez[1], J.A.M Green[2], L. Pan[1], H. Han[1], and N.R. Golledge[3]

[1]Department of Earth and Planetary Sciences, McGill University, Montreal, QC, Canada

[2]School of Ocean Sciences, Bangor University, Menai Bridge, Gwynedd, United Kingdom

[3]Antarctic Research Centre, Victoria University of Wellington, Wellington 6140, New Zealand

Corresponding author: Anna-Mireilla Hayden (anna-mireilla.hayden@mail.mcgill.ca)

*now at: Department of Geography and Environmental Management, University of Waterloo, Waterloo, ON, Canada

Key Points:

- We model future sea level and tide changes in Hudson Bay, Canada due to continental ice loss from past and present ice sheets.
- The magnitude and sign of future sea level and tide changes in Hudson Bay depend on the evolution of the Antarctic Ice Sheet.
- Water depths in Hudson Bay could increase by 14.5 meters by 2500 if the Antarctic Ice Sheet undergoes rapid retreat.

Abstract

Past and modern large-scale ice sheet loss results in geographically variable sea level changes. At present, in Hudson Bay, Canada, sea level is decreasing due to glacial isostatic adjustment, which represents a departure from the globally averaged sea level rise. However, there are large uncertainties in future sea level trends with further polar ice sheet retreat in the coming centuries. Sea level changes affect ocean tides considerably because tides are highly sensitive to changes in bathymetry. Here, we present multi-century sea level projections associated with a suite of past and future ice loss scenarios and consider the impact of these changes on ocean tides using an established tidal model. Modern tides in Hudson Bay are poorly resolved due to large uncertainties in bathymetry. To establish an initial condition for our simulations, we constrain bathymetry in the bay using tide observations. Due to gravitational, Earth rotational and deformational effects, Greenland ice loss will produce a small sea level fall in the bay, while Antarctic ice loss will produce a larger than average sea level rise. Our results show that the response of the Antarctic Ice Sheet to climate change strongly impacts the magnitude and sign of future sea level and tidal amplitude changes in the region, with the largest changes predicted in Hudson Strait and Foxe Basin. We emphasize that further constraints on bathymetry and accurate projections of sea level and tides in Hudson Bay are imperative for assessing the associated impacts on coastal communities and ecosystems.

Plain Language Summary

Hudson Bay is a shallow bay in northern Canada surrounded by coastal communities and ecosystems that are vulnerable to future sea level change. The bay was ice covered 21,000 years ago, and sea level is currently falling there due to ongoing land uplift since the ice retreated. It is unclear if this trend will continue as the Greenland and Antarctic Ice Sheets melt, contributing to spatially variable sea level changes. Sea level changes also impact ocean tides due to their sensitivity to water depth. We model future sea level and tide changes in the Hudson Bay region associated with land uplift and projections of Greenland and Antarctic ice loss over the next 500 years. With less Antarctic ice loss, sea level continues to fall and tidal amplitudes decrease. Conversely, high-end projected Antarctic ice loss could increase water depths in Hudson Bay by up to 14.5 meters by 2500 and tidal amplitude changes could exceed 1 meter, increasing in much of Hudson Bay while decreasing in Hudson Strait. A better understanding of the response of Antarctica to climate change will improve projections of sea level and tide changes in the Arctic and the associated societal and environmental impacts.

1. Introduction

Global mean sea level rise has accelerated in recent decades (Chen et al., 2017; Hay et al., 2015; Nerem et al., 2018), and this acceleration is expected to continue as global temperatures rise, resulting in thermal expansion of the oceans and melting of mountain glaciers and the polar ice sheets (Church et al., 2013; Clark et al., 2015; Slangen et al., 2016). Of these contributors, the Greenland and Antarctic Ice Sheets hold the largest potential to increase global mean sea level (WRCP Sea Level Working Group, 2018), and are expected to be the dominant contributors to global mean sea level rise on multi-century timescales (Church et al., 2013; Golledge et al., 2015). Regional sea level changes associated with ice loss can differ substantially from the global mean, due to gravitational, Earth deformational, and rotational effects (e.g. Clark & Lingle, 1977; Gomez et al., 2010; Mitrovica et al., 2001). Furthermore, past (ice age) ice cover changes lead to ongoing glacial isostatic adjustment (GIA) that contributes to regional variability in sea level change. GIA effects can be considerable in regions such as the Hudson Bay Complex (HBC, defined here as Hudson Bay, James Bay, Foxe Basin and Hudson Strait, Figure 1a) in northern Canada that were once ice covered during the Last Glacial Maximum. In the HBC, sea level is presently falling due to GIA, but it is unclear if this trend will continue in the coming centuries due to the large uncertainties in the future evolution of the polar ice sheets, in particular the Antarctic Ice Sheet (e.g. Church et al., 2013; DeConto & Pollard, 2016; Golledge et al., 2015).

Here, we define sea level as the height of the sea surface relative to the solid Earth surface, or equivalently, ocean bathymetry. Global and regional patterns of sea level change have been shown to have a strong influence on ocean tides (e.g., Padman et al. 2018; Wilmes et al., 2017), because tides travel as shallow water waves, which are sensitive to ocean bathymetry. Changes in ocean bathymetry (caused by changes in sea surface height and/or the shape of the sea floor) can lead to changes in tidal wave propagation speed, energy dissipation, and amplitudes (Green, 2010). Variations in sea level and the associated changes in ocean tides can, in turn, affect other coastal processes and ecosystems such as the development of salt marshes, coastal erosion, frequency and magnitude of flood events, and saltwater intrusion of surface water (Craft et al., 2009; Kirwan & Guntenspergen, 2010; Kirwan et al., 2010; Kirwan & Megonigal, 2013; Nicholls & Cazenave, 2010; Ross et al., 2017). Finally, Arctic and sub-Arctic indigenous communities surrounding the HBC are among the most vulnerable to climate change (IPCC, 2014), with their livelihoods and food sources critically impacted by coastal changes (e.g. Lemmen et al., 2016; Tsuji et al., 2009, 2016).

Projections of future sea level change in the HBC due to climate change have been relatively limited. Gough (1998) suggested that sea level in Hudson Bay could begin to increase in the current century as the global mean sea level rise associated with climate change outpaces the sea level fall due to glacial isostatic uplift. However, Gough's simple model did not capture the spatial variability in sea level change that arises from melting current ice sheets. More recently, Tsuji et al. (2009, 2016) and Lemmen et al. (2016) calculated the spatially variable sea level change and suggested that glacial isostatic uplift would persist in parts of the HBC in the coming centuries but did not consider a wide range of possible climate-driven sea level changes. Recent work has shown that even under the same climate forcing scenario, Representative Concentration Pathway (RCP) 8.5, projections of Antarctica's contribution to global mean sea level rise range from 2.25 m to 15.65 m by 2500 (DeConto & Pollard, 2016; Golledge et al., 2015, 2019). Given this large uncertainty, it is unclear what the dominant contributor to sea level change in the HBC will be, or even what the sign of sea level change will be. Furthermore, due to the relatively shallow bathymetry in the HBC, and the low-lying topography that surrounds the bay (Figure 1a), a small rise or fall in sea level will result in a large shoreline migration, amplifying the HBC's sensitivity to uncertainty in future sea level change.

Previous regional studies have investigated future sea level and tide changes on the European Shelf (e.g., Idier et al., 2017; Pelling & Green, 2014; Pickering et al., 2012), the Patagonian Shelf (Carless et al., 2016), the Gulf of Maine (Pelling & Green, 2013), the Gulf of Mexico (Passeri et al., 2016), and the Bohai Sea in China (Pelling et al., 2013), but studies of the HBC are lacking. The HBC is a particularly interesting region with regards to ocean tides. The tidal range of Ungava Bay in Hudson Strait (16.8 m ± 0.2 m, Drinkwater, 1986), rivals that of the Bay of Fundy (17.0 m ± 0.2 m, O'Reilly et al., 2005), as the region with the largest tidal range in the world. Furthermore, Egbert & Ray (2001) found that more tidal energy is dissipated in the HBC alone than in any other region in the world. This is because the HBC is near resonant at the semi-diurnal tidal forcing frequency (Arbic et al., 2007; Webb, 2014), producing large semi-diurnal tides (exceeding 4 m amplitudes in some areas, Figure 1b) that are further amplified due to the HBC's location on a continental shelf (Clarke & Battisti, 1981). The resonant properties of the HBC and its shallow continental shelf sea character can strongly influence deep ocean tides in the connecting Atlantic Ocean (Arbic et al., 2009; Arbic & Garrett, 2010), so any large-scale change in the HBC can have consequences far away from the region. Previous work on paleotides in the region indicated a strong sensitivity of ocean tides to changes in sea level (Arbic et al., 2004; Egbert et al., 2004; Uehara et al., 2006). However, modern tides in the HBC are not well resolved due to limited bathymetry data that can be used to constrain models (Egbert & Ray, 2001). Projecting future tides therefore requires, as a first step, an appraisal of the performance of available bathymetry models in reproducing modern tides in the HBC.

Wilmes et al. (2017) showed that a future complete collapse of the Greenland and West Antarctic ice sheets would strongly impact tides globally, and that simulations that take into account spatial variability in sea level change differ substantially from those that assume the global average equivalent rise. In particular, in Hudson Bay, the spatially variable sea level change associated with Greenland ice loss is opposite in sign to the uniform global average sea level rise scenario, which, in turn, results in large differences in predicted tidal changes. Furthermore, they show that spatially variable changes in sea level, and in turn tidal amplitudes in much of the HBC are positive under West Antarctic ice sheet collapse and negative under Greenland ice sheet collapse.

As a complete collapse of the Greenland and West Antarctic ice sheets represents a long term, upper bound on their contribution to sea level change, a question arises: How will future sea level and tides in the HBC evolve under combined, transient melting of the ice sheets in the coming centuries? Greenland's contribution to sea level change, which is not expected to exceed 20 cm of global mean sea level equivalent by 2100 (Church et al., 2013; IPCC, 2019), is predominantly driven by surface mass balance, followed by ice discharge via icebergs (Church et al., 2013; IPCC, 2019). The HBC is relatively insensitive to Greenland ice loss due to its close proximity to the net-zero sea level change line associated with gravitational effects that arise from Greenland melting. Conversely, the dynamic response is expected to dominate sea level changes due to Antarctic ice loss, but the future contribution from Antarctica remains highly uncertain due to the lack of observations to constrain models and an incomplete description of ice sheet-ocean-atmosphere interactions in current models (Kopp et al. 2017; IPCC, 2019). Projections range from tens of centimeters to more than 10 m global mean sea level equivalent over multi-century timescales (e.g., Golledge et al., 2019; Pollard et al., 2017). In contrast to Greenland melting, gravitational effects due to Antarctic ice loss will lead to a larger-than-global-average sea level rise in the HBC. Here, we investigate to the opposing influence of gravitational effects and the large uncertainty in Antarctic projections on sea level and tide changes in the HBC. We consider a single contribution from the Greenland Ice Sheet and low- and high-end possible contributions to sea level change from the Antarctic Ice Sheet under RCP8.5 climate warming. On decadal timescales, sea level changes will likely be dominated by GIA, but on centennial timescales, the contribution from ice sheets could exceed GIA, in particular under high-end warming scenarios. This transition from a regime of sea level fall to one of rise, and the associated changes in tides, is important to consider in assessing coastal climate change impacts and develop adaption strategies.

The paper is structured as follows. In section 2, we describe the ice loss and sea level projections and the tide model setup. Due to the sensitivity of tides to bathymetry, we discuss constraints on modern bathymetry in the HBC in section 3 and present a bathymetry model that improves modern non-assimilative tide simulations. In section 4, we present predictions of future sea level changes associated with future retreat of the polar ice sheets and ongoing GIA and the associated tidal changes in the HBC. We conclude with a discussion in section 5.

2. Methods

2.1 Sea level and ice sheet modelling

We adopt the sea level theory from Kendall et al. (2005) and Gomez et al. (2010) to predict the spatially variable sea level changes resulting from past and future ice cover variations using a gravitationally self-consistent sea level model that incorporates viscoelastic deformation of the solid earth due to surface ice and ocean mass loading, migrating shorelines, and Earth rotational effects. Elastic and density structure of the solid Earth in all simulations is provided by the Preliminary Reference Earth Model (PREM) (Dziewonski & Anderson, 1981) and viscosity structure is given by the VM2 Earth model (Peltier, 2004) unless otherwise specified. The modern topography that serves as input to the sea level model is taken from GEBCO 2014 (Weatherall et al., 2015) globally, with the composite regional bathymetry described below over the HBC. All calculations are performed up to spherical harmonic degree 512.

We simulate the future evolution of the polar ice sheets in Greenland and Antarctica with dynamic ice sheet models. We focus on projections adopting RCP 8.5 (Collins et al., 2013), representing the business-as-usual emissions scenario as it serves as the upper bound of expected global temperature increase, and hence contribution of the ice sheets to sea level change in the HBC. Furthermore, by considering a single RCP scenario, we highlight the variability that emerges among ice loss and sea level projections that are guided by the same emissions framework.

Greenland and Antarctic ice thickness projections are generated using the Parallel Ice Sheet Model (PISM) version 0.7.3, a hybrid ice model with shallow shelf-shallow ice approximations for floating and grounded ice (Winkelmann et al., 2011). Following the procedure outlined in Golledge et al. (2019), future climate forcing on the ice sheets is driven by the Coupled Model Inter-comparison Project Phase 5 (CMIP5) multi-model ensemble mean outputs. The ice sheet model simulations are performed on a high-resolution (2.5 km for Greenland and 5 km for Antarctica) polar stereographic grid. We apply a Gaussian smoothing filter on the changes in total (floating and grounded) ice thicknesses, then interpolate ice thickness predictions onto a lower resolution Gauss-Legendre 512 x 1024 global grid, to serve as input to the sea level model. We consider the Antarctic projection from Golledge et al. (2019) as the low-end projection of future Antarctic ice loss under RCP8.5 (henceforth the “low-end” scenario). We also consider an alternative simulation for the Antarctic Ice Sheet that predicts much greater ice loss under RCP8.5. This high-end projection of Antarctic ice thickness changes (hereafter referred to as the “high-end” scenario) is provided by a simulation in Pollard et al. (2017) using a coupled ice sheet – sea level model that includes ice cliff and hydrofracturing physics and a hybrid combination of shallow ice-shallow shelf approximations for ice dynamics. Ice thickness variations are provided by the ice model at 20 km resolution and then linearly interpolated onto the global 512 x 1024 grid.

To fully quantify the sea level changes in Hudson Bay, we also incorporate the contribution of ongoing GIA associated with past ice cover changes over the last deglaciation, which, in our simulations, spans the time period of 21,000 years ago to the year 2000 (henceforth the modern). We model ice loading changes over the last deglaciation by adopting the ICE-5G ice history with the VM2 Earth model (Peltier, 2004) and the ICE-6G ice history with the VM5a Earth model (Argus et al., 2014; Peltier et al., 2015). Each simulation was run from 21,000 years ago to 500 years in the future, and the predictions of change from the modern to the year 2500 were added to the sea level changes associated with future ice sheet retreat described above (see Figure S1 for a comparison of ICE-5G and ICE-6G).

The total sea level change is calculated as the sum of the contributions from Greenland, Antarctica, and GIA. Note that our projections do not include oceanographic effects. In the current century, these are expected to contribute a relatively uniform sea level rise in the bay under future climate warming (Jevrejeva et al., 2016), but the magnitude, timing and spatial variability of these changes is challenging to simulate in the HBC on multi-century timescales. While these effects would alter the timing of the change from a sea level fall to a sea level rise, they would likely not offset the overall effect of transitioning from a sea level fall to a sea level rise. In addition, the size of the contribution is well within the range of Antarctic contributions considered here. Shorter timescale simulations should include the influence of ocean dynamics on sea level and tides.

2.2 Tide modelling

We use the Oregon State University Tidal Inversion Software (OTIS) (Egbert et al., 1994; 2004) to model present-day and future tides in Hudson Bay. OTIS solves the linearized shallow water equations forced by the tidal potential and with energy dissipation from bed friction and parameterized tidal conversion (e.g., Green & Nycander 2013; see Wilmes et al., 2017 for details on the model setup).

The HBC tide model was run at 1/30° x 1/30° horizontal resolution and simulated the tidal constituents M_2, S_2, and K_1. The extent of the model domain is shown in Figure 1. Dissipation of tidal energy was calculated according to Egbert and Ray (2001; see also Wilmes et al., 2017 for a detailed description). For the present-day simulations, TPXO8 (Egbert & Erofeeva, 2002; see http://volkov.oce.orst.edu/tides/tpxo8_atlas.html for the latest version) elevations were used as forcing at the open boundaries. TPXO8 is an observation constrained tide model solution that assimilates tide gauge observations and satellite altimetry to produce a highly accurate estimate of the tides (~2 cm RMS error compared to un-assimilated tide gauge data; see Egbert & Erofeeva, 2002, and Stammer et al., 2014 for details).

For the future tide simulations, sea level change predictions described in section 2.1 are added to the present-day bathymetries for both HBC and the global setup. Simulations are performed for 2100, 2300, and 2500 under low-end and high-end Antarctic contributions. Elevation changes in response to each of the future sea level change scenarios simulated by a near-global (86° S - 89° N) tidal model (see next paragraph) were added to the boundary conditions used for the present-day simulations, thereby ensuring a high degree of accuracy for high-resolution HBC future simulations. We carry out two sets of runs for each time slice: one where flooding of low-lying land is permitted (denoted ‘flood’) and a second one where flooding is not permitted (‘no-flood’).

The near-global tide model simulations were also run with OTIS (see Wilmes et al., 2017 for details on linearized shallow wave equations, and internal drag and SAL parameterizations). The underlying bathymetry is RTopo-2 (Schaeffer et al., 2016) and the model is run at 1/8° x 1/8° horizontal resolution for 21 days to simulate M_2, S_2 and K_1. The M_2 amplitude errors when compared to TXPO8 are 5.6 cm globally and 2.8 cm in the deep ocean (see Table S1). Integrated M_2 tidal dissipation for the global and deep ocean is within 6 % and 7 %, respectively, of values computed for TPXO8, despite the very different resolutions in the shelf seas (TXPO8 has a resolution of 1/30 degree in most shelf seas; see also Egbert and Ray, 2001). Simulations using the same sea level scenarios as for the regional model were carried out with the near-global model and used as boundary conditions for the regional model simulations. Land-ocean boundaries in this case were kept constant (i.e., land was not permitted to flood) due to the low resolution of the model.

3. Constraining Modern Bathymetry

Numerical prediction of tides in near-resonant basins, such as Hudson Bay, are strongly sensitive to the adopted ocean bathymetry (Egbert & Ray, 2001; Green, 2010; Padman et al. 2018). Therefore, in order to project future tide changes, we require an accurate estimate of modern bathymetry. Bathymetry in the HBC is poorly constrained due to the sparsity of available data, related to the HBC's shallow depths, spatial extent, and limited commercial shipping routes. Furthermore, there is substantial disagreement between global bathymetry datasets in the HBC (Figure S2); differences between datasets reach up to 200 m in some areas of the complex. As a result, tide models struggle to accurately capture the tides in the region.

Given the lack of available data to distinguish between these bathymetry models, we seek to simultaneously find a bathymetry to use for (future) projections and to improve non-assimilative modelling of the modern tides in HBC. To do this, we simulate modern tides in the HBC using the configuration described in 2.2 with a suite of different bathymetry models GEBCO 2008 (see The GEBCO_2008 Grid, version 20100927, www.gebco.net), GEBCO 2014 (Weatherall et al., 2015), ETOPO1 (Amante & Eakins, 2009), and SRTM30_Plus (Becker et al., 2009) and evaluate their performance, focusing on Hudson Bay and Strait.

Figure 2a-d shows the difference between the simulated M_2 tidal amplitudes using the four bathymetry datasets considered (ETOPO1, GEBCO 2008, SRTM30_Plus, and GEBCO 2014) and the TPXO8 amplitudes. We calculate the root mean square complex elevation errors (RMSEs) against 14 tide gauges (see Text S1 for details and Figure 2 for their locations), TPXO8 and TPXO9 (see https://www.tpxo.net/global/tpxo9-atlas for details and the latest version) to evaluate the performance of bathymetry models in reproducing modern tides over the global domain (see Table 1 for a quantification of the errors). Amplitude and phase RMSEs are shown in Tables S2 and S3 for all ocean depths (total RMSE) and deep oceans regions (water depths > 500 m, deep RMSE).

The simulation using ETOPO1 produced the largest elevation and amplitude errors of all the simulations (Figure 2a and Table 1), with amplitudes differing from TPXO8 by more than 1 m in Hudson Strait and James Bay. Both GEBCO 2008 (Figure 2b) and GEBCO 2014 (Figure 2d) perform well in Hudson Strait, each with mean amplitude differences of 21 cm and 15 cm in Hudson Strait, respectively. In Hudson Bay, SRTM30_Plus (Figure 2c) matches more closely than the GEBCO simulations, differing from TPX08 with a basin amplitude RMSE of 7 cm. The largest amplitude errors in all simulations are in Hudson Strait, where there are also the largest differences in depths between datasets (Figure S2) and the largest tidal amplitudes (Figure 1b).

To improve the accuracy of our non-assimilative tidal simulations, we develop a composite bathymetry (Figure 2e) based on how well each existing bathymetry dataset performed regionally in the comparison to TPXO8 in the HBC. Our composite bathymetry merges, using linear weighting, SRTM30_Plus bathymetry in Hudson Bay and GEBCO 2008 bathymetry elsewhere in the HBC. The amplitudes of the tide simulation adopting the composite bathymetry differ from TPX08 in Hudson Bay on average by 6 cm. The largest amplitude errors in James Bay and Foxe Basin are less than ± 25 cm, with mean errors of 5 cm and 13 cm, respectively. Our composite bathymetry improves the amplitude fit in Hudson Strait, with an average amplitude difference of 20 cm when compared to TPXO8. Furthermore, we find that our composite, regional bathymetry substantially reduces elevation errors both in comparison to tide gauges, TXPO8 and TXPO9 (Table 1) and also both total and deep RMSE for amplitudes and phases (Table S3) for all simulated constituents. Consequently, we adopt this composite, modern bathymetry in the future sea level and tide projections shown in the sections to follow.

4. Results

4.1 Sea level change

Figure 3 shows the projected contributions to sea level change in the HBC associated with GIA and melting from the Greenland Ice Sheet and Antarctic Ice Sheet for the three time slices 2100, 2300 and 2500. The contribution from GIA (Figure 3a-c) shows a sea level fall across the HBC. James Bay and Churchill, Manitoba regions experience the maximum predicted sea level fall (see Figure 1a), with a magnitude of 1.2 m in both regions by 2100, and 5.9 m and 5.7 m respectively, by 2500. In Foxe Basin, sea level fall associated with GIA reaches 0.9 m by 2100, and 4.3 m by 2500. The sea level fall is driven by the larger thickness of the Laurentide Ice Sheet during the Last Glacial Maximum in these regions and the later termination of deglaciation. Hudson Strait sees a more moderate fall of 0.3 m by 2100 and 1.5 m by 2500. In contrast, to the east of the HBC in Davis Strait region, sea level rises over the 500-year GIA simulation (red regions in Figure 3a-c) due to the subsidence of peripheral bulges that formed around the ice sheets at the Last Glacial Maximum in our ICE-5G simulation.

Next, we consider the contribution from melting of the polar ice sheets (Figure 3d-l). There are a number of physical effects contributing to the differences in sea level change in the HBC associated with Greenland (Figure 3d-f) and Antarctic (Figure 3g-l) ice loss. An ice sheet exerts a gravitational attraction on the surrounding water, and this attraction weakens as the ice sheet loses mass, resulting in a local sea level fall within ~2000 km of the ice loss (Woodward, 1888). At greater distances from the source of ice loss, sea level rises more the global average (Tamisiea & Mitrovica, 2011). Viscoelastic uplift of the solid Earth in and around the region of ice loss further accentuates the local sea level fall, and deformation of the Earth due to loading of the oceans with water and changes in the planet's rotation associated with surface mass redistribution add geographic variability to the sea level change farther away from the ice sheet. In our simulations, the Greenland Ice Sheet is projected to contribute 0.10 m and 0.55 m of global averaged sea level rise by 2100 and 2500, respectively, but the HBC is within the zone of gravity-driven sea level fall for the Greenland Ice Sheet. Therefore, Greenland melting is projected to contribute a low amplitude drop in sea level across the HBC that decreases in amplitude with distance from Greenland. The smallest sea level decrease occurs in the south-eastern part of the HBC (Figure 3d-f and Figure S3a) and the largest sea level fall can be seen in northern Foxe Basin (up to 0.7 m by 2500) and the northern Labrador Sea. In Hudson Strait, the projected sea level decrease reaches 0.5 m by 2500. Central Hudson Bay would experience up to a 0.2 m decrease in sea level by 2500. In James Bay, sea level remains unaltered by 2100, with a shift to a sea level rise by 2500 that does not exceed 0.10 m. The sea level fall due to Greenland melting is an order of magnitude smaller than that caused by GIA. Sea level in the HBC is hence relatively insensitive to Greenland ice loss due to the fingerprint pattern and the proximity of the southern and western coasts of the HBC to the region of net-zero sea level change.

Melting from the Antarctic Ice Sheet, on the other hand, would lead to a sea level rise in the HBC that is approximately 1.2 times greater than the global mean sea level equivalent rise associated with the melting, with a relatively uniform rise across the HBC (Figure S3b). Figure 3g-l show projected sea level changes in response to the low-end (Figure 3g-i) and high-end (Figure 3j-l) responses of the Antarctic Ice Sheet to the RCP8.5 scenario. Under the low-end simulation, Antarctic melting would lead to a maximum sea level rise in the HBC of 0.1 m by 2100 and 2.1 m by 2500. The high-end scenario (j-l) predicts an order of magnitude larger sea level rise of up to 0.8 m by 2100 and 14.5 m by 2500 across the HBC.

In Figure 4, we consider the sum of all the contributions shown in Figure 3 (see also Figure S4 for the total sea level change adopting ICE-6G). Under the low-end Antarctic ice loss scenario (Figure 4a-c), the sea level change at 2100, 2300, and 2500 is dominated by GIA effects. The largest sea level decreases are predicted in the regions where the signal from GIA is greatest (Figure 3a-c). At 2100 (Figure 4a), the magnitude of sea level fall ranges from 1.1 m in Churchill to 1.2 m in James Bay. In Hudson Strait, the amplitude of sea level fall is damped and on the order of 0.4 m. East of Hudson Strait in the Davis Strait, a slight rise is seen, where Antarctic ice loss and GIA are both contributing a sea level rise. By 2300 (Figure 4b), the sea level fall ranges from 1 m in central Hudson Bay up to 2.75 m in James Bay. Ungava Bay, at the entrance of Hudson Strait, is the only area in the HBC that experiences a sea level rise, reaching up to 0.4 m. Thus, despite that the largest sea level fall due to Greenland ice loss is predicted in the Hudson Strait (Figure 3d-f), in addition to the contribution from GIA, the rise associated with Antarctic ice loss is not compensated for. By 2500, the sea level fall across much of the HBC reaches 3 m. Our low-end simulation suggests a gradual extension of sea level rise into the HBC. By 2500, the extent of sea level rise spreads westwards from the Hudson Strait into Hudson Bay, where sea level rise is less than 0.5 m.

The projection that incorporates the high-end Antarctic scenario is characterized by a transition from sea level fall to sea level rise across the HBC over the simulation time. At 2100 under this high-end Antarctic scenario (Figure 4d), GIA still dominates in Hudson Bay, James Bay and northern Foxe Basin. In other regions of the HBC, the signal of sea level rise from Antarctic ice loss already begins to outpace the signal from GIA by 2100. We find that by 2200 sea level has begun to rise across the entire HBC. Despite the large GIA signal in Foxe Basin and James Bay, our projections indicate that these regions would experience up to 3 m of sea level rise by 2200 and that sea level rise in other regions in the HBC reaches up to 4.5 m. In 2300 (Figure 4e), a maximum sea level rise of 9.5 m is predicted in Ungava Bay in Hudson Strait, with the smallest rise of 6.3 m in James Bay. The magnitude of minimum sea level rise under the high-end scenario at 2300 is triple the magnitude of maximum sea level fall predicted from the low-end scenario. At 2500 (Figure 4f), sea level rise exceeds 14 m in some regions of Hudson Strait. In Foxe Basin, the projected 10 m rise by 2500 represents, on average, a 10 % increase in water depth, relative to present day. Moreover, the 9 m rise predicted for James Bay suggests a 20 % increase in water depth relative to present day. As in 2300, we find that the magnitude of minimum sea level rise in James Bay and Foxe Basin under the high-end scenario in 2500 is three times the magnitude of maximum sea level fall calculated from the low-end scenario.

4.2 Tides

In Figure 5, we present the M_2 tidal amplitude changes associated with the total sea level changes shown in Figure 4. The tidal M_2 amplitude responses differ substantially between the low-end (Figure 4a-c) and high-end (Figure 4d-e) Antarctic ice loss scenarios. For the low-end scenarios, all three time slices show a similar amplitude change pattern with changes increasing in magnitude from 2100 to 2500. Both the flood (Figure 5) and no-flood (Figure S8) runs show very similar amplitude change characteristics, therefore the description will be based on the simulations permitting flooding. Amplitudes increase in Hudson Strait and in the western half of Foxe Basin whereas decreases can be seen along most of the Hudson Bay margins.

Under the low-end scenario and in Foxe Basin, where sea level deceases by ~1 m in 2100 and by over 2 m in 2300 and 2500, respectively, occur, the amphidrome in the eastern part of the bay is shifted eastward due to increases in the energy fluxes into the eastern part of the bay (see panels a-c in Figures S9 and S10). Small decreases in the energy fluxes along the western margin of Hudson Bay can be seen which are associated with a small shift of the western amphidrome towards the western margin, thus decreasing amplitudes. The eastern amphidrome shifts north-eastward leading to deceases in amplitudes along the eastern margin. In James Bay, the amphidrome in the east moves eastward and becomes degenerate, leading to increases in amplitudes in the south-east part of the bay.

For the simulations adopting the high-end Antarctic ice loss scenario, the changes for the 2100 simulation are small and will therefore not be discussed. For the 2300 and 2500 high-end scenarios (as in the low-end scenarios), the flood and no-flood responses are very similar. However, in the no-flood simulations the amplitude changes are larger, especially along the eastern margins of Hudson Bay and Foxe Basin (see Figure S8). In the flood runs, for both 2300 and 2500 (see panels e and f in Figures 5 and S8), large amplitude decreases can be seen in Hudson Strait (exceeding 70 cm by 2500), in Ungava Bay and in the southern and northern parts of Foxe Basin (exceeding 1 m by 2500 in both regions). In eastern Foxe Basin and along the eastern margins of Hudson Bay, amplitudes increase by around 20-30 cm by 2500, whereas along the south-eastern margins of Hudson Bay amplitudes decrease by approximately the same amount.

The amplitude decreases in Hudson Strait for 2300 and 2500 high-end Antarctic ice loss scenarios exceed 25 % and are associated with a strong decrease in energy fluxes through Hudson Strait and into Foxe Basin (see panels e and f in Figures S9 and S10). The decrease in energy fluxes together with increases in energy losses in the newly flooded areas around the margins of Foxe Basin shift the eastern amphidrome in Foxe Basin southward, thus increasing amplitudes in the easternmost part of the basin and decreasing amplitudes in the south. Similarly, energy fluxes along the western margins of Hudson Bay decrease, shifting both amphidromes westward and increasing amplitudes in the east of the bay. In James Bay, the decreased energy flux shifts the amphidrome north-westward increasing amplitudes in the south east of the bay and leading to decreases in the western half.

Next we consider the impact on energy dissipation. For the low-end simulations, integrated dissipation over the area of HBC remains similar to present (Table S8). In the no-flood runs, dissipation remains constant at the present-day value of 232 GW with increases and decreases in Foxe Basin cancelling each other out in all three time-slices. In the flood runs, total dissipation increases by 5 % in the 2500 time slice. For the high-end scenarios, in contrast, the changes are much larger. In the no-flood runs, integrated dissipation of the HBC decreases by 23 % by 2300 and 40 % by 2500. Nearly all of the decreases in dissipation are due to reduced energy losses in Foxe Basin, Hudson Strait and Ungava Bay. In the 2500 time-slice, these three areas together experience a drop in dissipation of ~80 GW which explains the majority of the dissipation decrease. For the flood runs, the dissipation change picture is very similar (see panels e and f in Figures S11 and S12), however, the integrated dissipation changes by only 3 and 7 % for 2300 and 2500, respectively. In these runs, the energy losses in the newly flooded areas nearly balance the dissipation losses away from the margins. However, if the newly flooded areas are excluded, the same large dissipation decreases in the three basins emerge (see last two columns of Table S8).

5. Discussion and Conclusions

We have provided the first regional study of future sea level changes in the Hudson Bay associated with ice loss from the Greenland and Antarctic Ice Sheets and GIA and their impact on ocean tides in the region. We showed that both sea level and tides in the HBC are relatively insensitive to Greenland melting but strongly sensitive to Antarctic Ice Sheet evolution, with our simulations indicating a transition from a sea level fall to a sea level rise across the HBC that is dependent on the adopted Antarctic ice loss scenario. In this work, we focused on the RCP8.5 emissions pathway, however more moderate warming scenarios such as RCP2.6 or RCP4.5 could prolong the duration of sea level fall in the HBC.

Our results indicate that the sea level fall associated with GIA contributes significantly to sea level change in the HBC and dominates under low-end Antarctic ice loss scenarios. HBC is dominated by sea level decreases (up to 1.2 and 3 m by 2100 and 2500, respectively). Hudson Strait is the only region that experiences sea level rise (up to 0.5 m by 2500). We found that the associated M_2 tidal amplitude changes are less than 0.2 m in the HBC by 2500, with tidal amplitude increases in Foxe Basin and western Hudson Strait, and tidal amplitude decreases across Hudson Bay, James Bay, and Ungava Bay in Hudson Strait. We have shown that small migrations of the amphidromic points are responsible for the observed changes in the M_2 tides.

Conversely, GIA does not compensate the projected sea level rise under more rapid Antarctic ice loss in our high-end scenario. In the projection adopting the high-end Antarctic ice loss scenario, sea levels begin to rise in much of the HBC by 2100, with a widespread transition from sea level fall to sea level rise by 2200 and reaching a peak sea level rise of 14.5 m in Ungava Bay in Hudson Strait by 2500. Under the high-end scenario, the M_2 tidal amplitude changes reach over 1 m with the largest decreases occurring in Hudson Strait and Foxe Basin and peak increases along the eastern margin of Hudson Bay by 2500. Furthermore, as the HBC is presently one of the areas on the planet where the most tidal energy is dissipated (Egbert & Ray, 2001) the significant decreases in dissipation in the open ocean areas of Hudson Strait, Foxe Basin and Ungava Bay (see panels d-f in Figures S11 and S12) suggested under our high-end scenario simulations could affect both local tidal mixing important for biogeochemistry but also the global tidal energy balance.

Our results suggest that the strong and uniform in sign responses of the Hudson Strait, Ungava Bay and Foxe Basin system to the sea level variations in both the high-end and low-end scenarios could be linked to the resonant properties of the basins. A number of previous studies have shown that the HBC straddles a number of resonant frequencies close to and either side of the M_2 frequency (Arbic et al., 2007, Cummins et al., 2010, and Webb, 2014). Our simulations show that Hudson Strait, Ungava Bay and Foxe Basin change in conjunction with each other in response to sea level changes. The moderate decreases in sea level (around 2 m) seen in the low-end scenario lead to increases in amplitudes, suggesting that the system is moving closer to a resonant state. In contrast, the increases in sea level seen in the high-end scenario in the 2300 and

2500 time slices drive strong amplitude decreases in Hudson Strait, Ungava Bay and Foxe Basin together with large decreases in dissipation. In the 2500 high-end simulations (both flood and no-flood), the dissipation decreases amount to around 80 GW when newly flooded areas are excluded, nearly halving the energy dissipated in the three basins with respect to present day.

Previous studies investigating resonances have generally considered Hudson Strait and Hudson Bay (together with Ungava Bay) as a resonant system (see e.g., Cummins et al., 2010). However, our results indicate that it is more likely that Foxe Basin and Hudson Strait together with Ungava Bay act as a near-resonant system at present; which, perturbed by sea level changes, exhibits large changes in amplitudes and dissipation. At present, in Foxe Basin ~110 GW of M2 tidal energy are dissipated, whereas in Hudson Bay a mere 20 GW are lost (see also Figure S13). Nearly half of the dissipation decreases in the 2500 high-end scenario occur in Foxe Basin, and the remainder take place in Hudson Strait and Ungava Bay. This hypothesis is supported by the pathway of the energy fluxes into the HBC (see Figure S14) and the changes thereof (Figures S9 and S10) (see also Figure 1 in Webb et al., 2014) where the main pathway of energy flow into HBC is through Hudson Strait and into the eastern part of Foxe Basin with very little energy transfer into Hudson Bay itself. A simple back of the envelope calculation of the natural period of Hudson Strait and Foxe Basin ($T = 4L/\sqrt{gD}$), using a distance L of 1600 km from outside the entrance of Hudson Strait to the south eastern margin of Foxe Basin and a mean depth D of 136 m, yields a resonant period T of 48.7 hrs, which is very close to four-times the M_2 period. A sea level decrease by 2 m as seen in the 2300 and 2500 low-end simulations increases the resonant period to 49.0 hrs, i.e. moving it closer to 4 times the M_2 period. In contrast, a sea level increase of 9 m and 13 m as in the 2300 and 2500 high-end simulations results in decreases in the resonant period to 47.1hrs and 46.5 hrs, respectively, thus moving away from four times the M_2 period.

We have carried out additional simulations with the same sea level forcing across HBC but with present-day boundary conditions at the open boundaries (not shown) and find very similar results as when we apply boundary conditions from the global model forced with sea level changes. A no-flood simulation of the high-end 2500 sea level change shows a dissipation decrease of 35 % which is very similar to the 40 % seen in our no-flood runs. We therefore conclude that, to a large extent, the changes seen in Hudson Bay, Ungava Bay and Foxe Basin are driven by changes in internal dynamics due the sea level changes rather than by external forcing outside our regional model domain. This is in contrast to, e.g., the work by Harker et al. (2019) carried out for the Australian Shelf.

Our HBC tidal runs performed at 1/30° degree resolution are more accurate than the global simulations shown in Wilmes et al. (2017) with a resolution of 1/8°. They found a global RMS error for M2 amplitudes of 7.7 cm (global) and 3.8 cm (deep) whereas our new global model setup has reduced errors of 5.6 cm (global) and 2.8 cm (deep). However, the responses to sea level changes in their simulations are similar to our findings for the HBC simulations. They compared tidal amplitude responses to non-uniform sea level changes due to full collapses of the West Antarctic Ice Sheet and the Greenland Ice Sheet and a uniform sea level rise of 12 m. The spatially variable sea level change scenario had a similar magnitude sea level fall over the HBC as the 2500 low-end scenario whereas the uniform sea level rise case was most akin to the 2500 high-end case shown here. The amplitude responses to the two different scenarios agree in their patterns between the two studies which increases our confidence in the results presented in Wilmes et al. (2017), despite the different model resolutions.

Here, we focused on the contributions due to ice mass loss from the polar ice sheets and GIA associated with the last deglaciation, however, oceanographic and sea ice changes in the HBC will also impact sea level and ocean tides, in particular on timescales shorter than the centennial timescales considered here. Thermal expansion and ocean dynamics are expected to contribute on the order of 0.3 m of sea level rise in the HBC under RCP8.5 by 2100 (Jevrejeva et al., 2016), similar to the contribution of these effects to globally averaged sea level rise of 0.21-0.33 m by 2100 estimated in the IPCC (Church et al., 2013). While regional estimates in the HBC are limited on multi-century timescales, the contribution of thermal expansion and ocean dynamics to globally averaged sea level rise under RCP8.5 is estimated to be between 0.29-1.81 m by 2300, and 0.37-2.77 m by 2500 (Church et al., 2013). We thus expect that the magnitude of oceanographic effects in the HBC will be smaller than the contributions from the Antarctic ice sheet and GIA (Figure 3) but could nonetheless impact the timing of the transition from sea level fall to sea level rise. Incorporating projections of variability in ocean dynamics would add to the work presented here, in addition to improving shorter term projections of sea level and tide changes in the HBC. Furthermore, we have considered changes in sea level and tides in the HBC during the ice-free season. Since Hudson Bay is currently characterized by a long sea ice cover season which dampens the magnitude of the tides (Godin, 1986; Kleptsova & Pietrzak, 2018; St-Laurent et al., 2008), future work will explore the impact of retreating sea ice on our results.

Previous simulations of modern tides have had large amplitude errors in the HBC (e.g. Wilmes et al., 2017) due to large uncertainty in the bathymetry in the HBC. Since bathymetry in the HBC is poorly constrained, we used tidal simulations and tide gauge data to constrain the bathymetry. We suggested that being able to simulate tides more accurately provides an indication of which bathymetry dataset is more accurate. We produced a composite bathymetry constrained using TPXO8 solutions and tide gauge observations that greatly improves the fit between predicted and observed modern tides, with total, and deep ocean root mean square errors around 12 and 3 cm, respectively. Our approach may be used to further refine bathymetry models in the Hudson Bay Complex and in other regions with sparse data. Our results also highlight the need for high-resolution bathymetry surveys in the HBC, a region that will become increasingly important as sea ice cover retreats and access via marine traffic increases in a warming climate. Furthermore, accurate bathymetry data has far-reaching implications for residents surrounding the HBC, including, for example, future land claim issues related to the formation of land bridges between islands and the mainland (Tsuji et al., 2016).

We emphasize that results from this research have profound impacts on ecosystems and communities surrounding the HBC. Due to the shallow topography and bathymetry in the HBC, we project that an increase in the absolute depth of water of up to 20 % could occur by 2500 under our high-end scenario, which would lead to changes in the extent of the intertidal zone and shoreline locations, in turn, affecting ecosystems including wetlands and marshes. If sea level rise outpaces the rate at which marshes grow, these areas will become inundated, reducing the capacity of these ecosystems to attenuate storm surges and flooding events (Kirwan & Guntenspergen, 2010). The substantial changes in dissipation and thus tidal mixing have the potential to impact water structure and biogeochemistry and thus primary and secondary productivity in HBC. Furthermore, the livelihoods, culture, and traditions of indigenous communities surrounding the HBC are inextricably linked to the natural environment. Coastal management and policy decisions should integrate the physical changes presented here. In doing so, these vulnerable groups will be better equipped to deal with future impacts of climate change on coastal regions.

We conclude that projections of changes in sea level and ocean tides in the HBC should take into account not only the sea level changes due to ongoing glacial isostatic adjustment from the past deglaciation, but also consider a range of spatially variable sea level change projections arising from land ice loss, in particular in Antarctica. Uncertainty in projections of change in coastal areas in the HBC is dominated by uncertainty in projections of the evolution of the Antarctic ice sheet. As our understanding of the response of Antarctica to climate change improves, so too will our projections of sea level and tide changes in the Arctic.

Acknowledgments, Samples, and Data

- The authors declare no conflicts of interest
- A.-M.H., N.G., H.H., and L.P. are funded by the Natural Sciences and Engineering Research Council of Canada, Canada Research Chairs, Canadian Foundation for Innovation and McGill University.
- S-B.W. and J.A.M.G acknowledge funding from the UK Natural Environment Research Council (MATCH, NE/S009566/1).
- N.R.G. is funded by contract VUW1501 from the Royal Society Te Aparangi and contract CO5X1001 from the Ministry for Business, Innovation and Employment.

- Topography and tidal amplitude data is available through the cited references. Model data would be made available to readers through a public repository upon publication.

References

Amante, C. & B.W. Eakins, 2009. ETOPO1 1 Arc-Minute Global Relief Model: Procedures, Data Sources and Analysis. NOAA Technical Memorandum NESDIS NGDC-24. National Geophysical Data Center, NOAA. doi:10.7289/V5C8276M

Arbic, B., & Garrett, C. (2010). A coupled oscillator model of shelf and ocean tides. *Continental Shelf Research*, *30*(6), 564-574. doi: 10.1016/j.csr.2009.07.008

Arbic, B., Karsten, R., & Garrett, C. (2009). On tidal resonance in the global ocean and the back-effect of coastal tides upon open-ocean tides. *Atmosphere-Ocean*, *47*(4), 239-266. doi: 10.3137/oc311.2009

Arbic, B., MacAyeal, D., Mitrovica, J., & Milne, G. (2004). Ocean tides and Heinrich events. *Nature*, *432*(7016), 460-460. doi: 10.1038/432460a

Arbic, B., St-Laurent, P., Sutherland, G., & Garrett, C. (2007). On the resonance and influence of the tides in Ungava Bay and Hudson Strait. *Geophysical Research Letters*, *34*(17). doi: 10.1029/2007gl030845

Argus, D., Peltier, W., Drummond, R., & Moore, A. (2014). The Antarctica component of postglacial rebound model ICE-6G_C (VM5a) based on GPS positioning, exposure age dating of ice thicknesses, and relative sea level histories. *Geophysical Journal International*, *198*(1), 537-563. doi: 10.1093/gji/ggu140

Becker, J., Sandwell, D., Smith, W., Braud, J., Binder, B., & Depner, J. et al. (2009). Global Bathymetry and Elevation Data at 30 Arc Seconds Resolution: SRTM30_PLUS. *Marine Geodesy*, *32*(4), 355-371. doi: 10.1080/01490410903297766

Carless, S., Green, J., Pelling, H., & Wilmes, S. (2016). Effects of future sea-level rise on tidal processes on the Patagonian Shelf. *Journal Of Marine Systems*, *163*, 113-124. doi: 10.1016/j.jmarsys.2016.07.007

Chen, X., Zhang, X., Church, J., Watson, C., King, M., & Monselesan, D. et al. (2017). The increasing rate of global mean sea-level rise during 1993–2014. *Nature Climate Change*, *7*(7), 492-495. doi: 10.1038/nclimate3325

Church, J.A., P.U. Clark, A. Cazenave, J.M. Gregory, S. Jevrejeva, A. Levermann, M.A. Merrifield, G.A. Milne, R.S. Nerem, P.D. Nunn, A.J. Payne, W.T. Pfeffer, D. Stammer and A.S. Unnikrishnan, 2013: Sea Level Change. In: Climate Change 2013: The Physical Science Basis. Contribution of Working Group I to the Fifth Assessment Report of the Intergovernmental Panel on Climate Change [Stocker, T.F., D. Qin, G.-K. Plattner, M. Tignor, S.K. Allen, J. Boschung, A. Nauels, Y. Xia, V. Bex and P.M. Midgley (eds.)]. Cambridge University Press, Cambridge, United Kingdom and New York, NY, USA.

Clark, J., & Lingle, C. (1977). Future sea-level changes due to West Antarctic ice sheet fluctuations. *Nature*, *269*(5625), 206-209. doi: 10.1038/269206a0

Clark, P., Church, J., Gregory, J., & Payne, A. (2015). Recent Progress in Understanding and Projecting Regional and Global Mean Sea Level Change. *Current Climate Change Reports*, *1*(4), 224-246. doi: 10.1007/s40641-015-0024-4

Clark, P., Shakun, J., Marcott, S., Mix, A., Eby, M., & Kulp, S. et al. (2016). Consequences of twenty-first-century policy for multi-millennial climate and sea-level change. *Nature Climate Change*, *6*(4), 360-369. doi: 10.1038/nclimate2923

Clarke, A., & Battisti, D. (1981). The effect of continental shelves on tides. *Deep Sea Research Part A. Oceanographic Research Papers*, *28*(7), 665-682. doi: 10.1016/0198-0149(81)90128-x

Collins, M., R. Knutti, J. Arblaster, J.-L. Dufresne, T. Fichefet, P. Friedlingstein, X. Gao, W.J. Gutowski, T. Johns, G. Krinner, M. Shongwe, C. Tebaldi, A.J. Weaver and M. Wehner, 2013: Long-term Climate Change: Projections, Commitments and Irreversibility. In: Climate Change 2013: The Physical Science Basis. Contribution of Working Group I to the Fifth Assessment Report of the Intergovernmental Panel on Climate Change [Stocker, T.F., D. Qin, G.-K. Plattner, M. Tignor, S.K. Allen, J. Boschung, A. Nauels, Y. Xia, V. Bex and P.M. Midgley (eds.)]. Cambridge University Press, Cambridge, United Kingdom and New York, NY, USA.

Craft, C., Clough, J., Ehman, J., Joye, S., Park, R., & Pennings, S. et al. (2009). Forecasting the effects of accelerated sea-level rise on tidal marsh ecosystem services. *Frontiers In Ecology And The Environment*, *7*(2), 73-78. doi: 10.1890/070219

Cummins, P. F., Karsten, R. H. & Arbic, B. K. (2010). The semi-diurnal tide in Hudson strait as a resonant channel oscillation. *Atmosphere-Ocean*, *48*(3), 163-176. doi: 10.3137/OC307.2010

DeConto, R., & Pollard, D. (2016). Contribution of Antarctica to past and future sea-level rise. *Nature*, *531*(7596), 591-597. doi: 10.1038/nature17145

Drinkwater, K. (1986). Chapter 13 Physical Oceanography of Hudson Strait and Ungava Bay. *Canadian Inland Seas*, 237-264. doi: 10.1016/s0422-9894(08)70906-1

Dziewonski, A., & Anderson, D. (1981). Preliminary reference Earth model. *Physics Of The Earth And Planetary Interiors*, *25*(4), 297-356. doi: 10.1016/0031-9201(81)90046-7

Egbert, G., Bennett, A., & Foreman, M. (1994). TOPEX/POSEIDON tides estimated using a global inverse model. *Journal of Geophysical Research*, *99*(C12), 24821. doi: 10.1029/94jc01894

Egbert, G., & Erofeeva, S. (2002). Efficient Inverse Modeling of Barotropic Ocean Tides. *Journal Of Atmospheric And Oceanic Technology*, *19*(2), 183-204. doi: 10.1175/1520-0426(2002)019<0183:eimobo>2.0.co;2

Egbert, G., & Ray, R. (2001). Estimates of M2 tidal energy dissipation from TOPEX/Poseidon altimeter data. *Journal Of Geophysical Research: Oceans*, *106*(C10), 22475-22502. doi: 10.1029/2000jc000699

Egbert, G., Ray, R., & Bills, B. (2004). Numerical modeling of the global semidiurnal tide in the present day and in the last glacial maximum. *Journal Of Geophysical Research: Oceans*, *109*(C3). doi: 10.1029/2003jc001973

Godin, G. (1986). Modification by an Ice Cover of the Tide in James Bay and Hudson Bay. *ARCTIC*, *39*(1). doi: 10.14430/arctic2048

Golledge, N., Keller, E., Gomez, N., Naughten, K., Bernales, J., Trusel, L., & Edwards, T. (2019). Global environmental consequences of twenty-first-century ice-sheet melt. *Nature*, *566*(7742), 65-72. doi: 10.1038/s41586-019-0889-9

Golledge, N., Kowalewski, D., Naish, T., Levy, R., Fogwill, C., & Gasson, E. (2015). The multi-millennial Antarctic commitment to future sea-level rise. *Nature*, *526*(7573), 421-425. doi: 10.1038/nature15706

Gomez, N., Mitrovica, J., Tamisiea, M., & Clark, P. (2010). A new projection of sea level change in response to collapse of marine sectors of the Antarctic Ice Sheet. *Geophysical Journal International*, *180*(2), 623-634. doi: 10.1111/j.1365-246x.2009.04419.x

Gough, W.A. 1998. Projections of sea-level change in Hudson and James Bays, Canada, due to global warming. Arctic and Alpine Research 30(1):84 – 88. doi: 10.2307/1551748

Green, J. (2010). Ocean tides and resonance. *Ocean Dynamics*, *60*(5), 1243-1253. doi: 10.1007/s10236-010-0331-1

Green, J., & Nycander, J. (2013). A Comparison of Tidal Conversion Parameterizations for Tidal Models. *Journal Of Physical Oceanography*, *43*(1), 104-119. doi: 10.1175/jpo-d-12-023.1

Hay, C., Morrow, E., Kopp, R., & Mitrovica, J. (2015). Probabilistic reanalysis of twentieth-century sea-level rise. *Nature*, *517*(7535), 481-484. doi: 10.1038/nature14093

Harker, A., Green, J. A. M., Schindelegger, M., & Wilmes, S.-B. (2019). The impact of sea-level rise on tidal characteristics around Australia. *Ocean Science*, *15*, 147–159. doi:/10.5194/os-15-147-2019

Idier, D., Paris, F., Cozannet, G., Boulahya, F., & Dumas, F. (2017). Sea-level rise impacts on the tides of the European Shelf. *Continental Shelf Research*, *137*, 56-71. doi: 10.1016/j.csr.2017.01.007

IPCC (2014). Climate Change 2014: Impacts, Adaptation, and Vulnerability. Summaries, Frequently Asked Questions, and Cross-Chapter Boxes. A Contribution of Working Group II to the Fifth Assessment Report of the Intergovernmental Panel on Climate Change [Field, C.B., V.R. Barros, D.J. Dokken, K.J. Mach, M.D. Mastrandrea, T.E. Bilir, M. Chatterjee, K.L. Ebi, Y.O. Estrada, R.C. Genova, B. Girma, E.S. Kissel, A.N. Levy, S. MacCracken,P.R. Mastrandrea, and L.L. White (eds.)]. World Meteorological Organization, Geneva, Switzerland, 190 pp.

IPCC (2019). Special Report on the Ocean and Cryosphere in a Changing Climate (SROCC) (2019); www.ipcc.ch/report/srocc.

Jevrejeva, S., Jackson, L., Riva, R., Grinsted, A., & Moore, J. (2016). Coastal sea level rise with warming above 2 °C. *Proceedings of The National Academy Of Sciences*, *113*(47), 13342-13347. doi: 10.1073/pnas.1605312113

Kendall, R., Mitrovica, J., & Milne, G. (2005). On post-glacial sea level - II. Numerical formulation and comparative results on spherically symmetric models. *Geophysical Journal International*, *161*(3), 679-706. doi: 10.1111/j.1365-246x.2005.02553.x

Kirwan, M., & Guntenspergen, G. (2010). Influence of tidal range on the stability of coastal marshland. *Journal of Geophysical Research: Earth Surface*, *115*(F2). doi: 10.1029/2009jf001400

Kirwan, M., & Megonigal, J. (2013). Tidal wetland stability in the face of human impacts and sea-level rise. *Nature*, *504*(7478), 53-60. doi: 10.1038/nature12856

Kirwan, M., Guntenspergen, G., D'Alpaos, A., Morris, J., Mudd, S., & Temmerman, S. (2010). Limits on the adaptability of coastal marshes to rising sea level. *Geophysical Research Letters*, *37*(23), n/a-n/a. doi: 10.1029/2010gl045489

Kleptsova, O., & Pietrzak, J. (2018). High resolution tidal model of Canadian Arctic Archipelago, Baffin and Hudson Bay. *Ocean Modelling*, *128,* 15-47. doi: 10.1016/j.ocemod.2018.06.001

Kopp, R., DeConto, R., Bader, D., Hay, C., Horton, R., & Kulp, S. et al. (2017). Evolving Understanding of Antarctic Ice-Sheet Physics and Ambiguity in Probabilistic Sea-Level Projections. *Journal of Geophysical Research: Earth's Future*, *5*(12), 1217-1233. doi: 10.1002/2017ef000663

Lemmen, D.S. and Warren, F.J. (2016): Synthesis; *in* Canada’s Marine Coasts in a Changing Climate, (ed.) D.S. Lemmen, F.J. Warren, T.S. James and C.S.L. Mercer Clarke; Government of Canada, Ottawa, ON, p. 17-26.

Mitrovica, J., Gomez, N., Morrow, E., Hay, C., Latychev, K., & Tamisiea, M. (2011). On the robustness of predictions of sea level fingerprints. *Geophysical Journal International*, *187*(2), 729-742. doi: 10.1111/j.1365-246x.2011.05090.x

Mitrovica, J., Tamisiea, M., Davis, J., & Milne, G. (2001). Recent mass balance of polar ice sheets inferred from patterns of global sea-level change. *Nature*, *409*(6823), 1026-1029. doi: 10.1038/35059054

Nerem, R., Beckley, B., Fasullo, J., Hamlington, B., Masters, D., & Mitchum, G. (2018). Climate-change–driven accelerated sea-level rise detected in the altimeter era. *Proceedings of The National Academy of Sciences*, *115*(9), 2022-2025. doi: 10.1073/pnas.1717312115

Nicholls, R., & Cazenave, A. (2010). Sea-Level Rise and Its Impact on Coastal Zones. *Science*, *328*(5985), 1517-1520. doi: 10.1126/science.1185782

O’Reilly, C. T., R. Solvason, and C. Solomon (2005), Where are the world’s largest tides?, in BIO Annual Report ‘‘2004 in Review,’’ edited by J. Ryan, pp. 44 – 46, Biotechnol. Ind. Org., Washington, D. C.

Padman, L., Siegfried, M., & Fricker, H. (2018). Ocean Tide Influences on the Antarctic and Greenland Ice Sheets. *Reviews of Geophysics*, *56*(1), 142-184. doi: 10.1002/2016rg000546

Passeri, D., Hagen, S., Plant, N., Bilskie, M., Medeiros, S., & Alizad, K. (2016). Tidal hydrodynamics under future sea level rise and coastal morphology in the Northern Gulf of Mexico. *Journal Geophysical Research: Earth's Future*, *4*(5), 159-176. doi: 10.1002/2015ef000332

Pelling, H., & Green, J. (2013). Sea level rise and tidal power plants in the Gulf of Maine. *Journal Of Geophysical Research: Oceans*, *118*(6), 2863-2873. doi: 10.1002/jgrc.20221

Pelling, H., & Green, J. (2014). Impact of flood defences and sea-level rise on the European Shelf tidal regime. *Continental Shelf Research*, 85, 96-105. doi: 10.1016/j.csr.2014.04.011

Pelling, H., Green, J., & Ward, S. (2013). Modelling tides and sea-level rise: To flood or not to flood. *Ocean Modelling, 63*, 21-29. doi: 10.1016/j.ocemod.2012.12.004

Pelling, H., Uehara, K., & Green, J. (2013). The impact of rapid coastline changes and sea level rise on the tides in the Bohai Sea, China. *Journal Of Geophysical Research: Oceans*, *118*(7), 3462-3472. doi: 10.1002/jgrc.20258

Peltier, W. (2004). Global glacial isostasy and the surface of the ice-age Earth: the ICE-5G (VM2) model and GRACE. *Annual Review of Earth and Planetary Sciences*, *32*(1), 111-149. doi: 10.1146/annurev.earth.32.082503.144359

Peltier, W., Argus, D., & Drummond, R. (2015). Space geodesy constrains ice age terminal deglaciation: The global ICE-6G_C (VM5a) model. *Journal of Geophysical Research: Solid Earth*, *120*(1), 450-487. doi: 10.1002/2014jb011176

Pickering, M., Wells, N., Horsburgh, K., & Green, J. (2012). The impact of future sea-level rise on the European Shelf tides. *Continental Shelf Research*, *35*, 1-15. doi: 10.1016/j.csr.2011.11.011

Pollard, D., Gomez, N., & Deconto, R. (2017). Variations of the Antarctic Ice Sheet in a Coupled Ice Sheet-Earth-Sea Level Model: Sensitivity to Viscoelastic Earth Properties. *Journal of Geophysical Research: Earth Surface*, *122*(11), 2124-2138. doi: 10.1002/2017jf004371

Ross, A., Najjar, R., Li, M., Lee, S., Zhang, F., & Liu, W. (2017). Fingerprints of Sea Level Rise on Changing Tides in the Chesapeake and Delaware Bays. *Journal of Geophysical Research: Oceans*, *122*(10), 8102-8125. doi: 10.1002/2017jc012887

Slangen, A., Adloff, F., Jevrejeva, S., Leclercq, P., Marzeion, B., Wada, Y., & Winkelmann, R. (2016). A Review of Recent Updates of Sea-Level Projections at Global and Regional Scales. *Surveys in Geophysics*, *38*(1), 385-406. doi: 10.1007/s10712-016-9374-2

Stammer, D., Ray, R., Andersen, O., Arbic, B., Bosch, W., & Carrère, L. et al. (2014). Accuracy assessment of global barotropic ocean tide models. *Reviews of Geophysics*, *52*(3), 243-282. doi: 10.1002/2014rg000450

Stewart, D.B., and Lockhart, W.L. (2005). *An Overview of the Hudson Bay Marine Ecosystem*. Canadian technical report of fisheries and aquatic sciences no. 2586. Retrieved from Government of Canada, Department of Fisheries and Oceans website: http://www.dfo-mpo.gc.ca/libraries- bibliotheques/toc-tdm/314704-eng.htm

St-Laurent, P., Saucier, F., & Dumais, J. (2008). On the modification of tides in a seasonally ice-covered sea. *Journal of Geophysical Research*, *113*(C11). doi: 10.1029/2007jc004614

Tamisiea, M., & Mitrovica, J. (2011). The Moving Boundaries of Sea Level Change: Understanding the Origins of Geographic Variability. *Oceanography*, *24*(2), 24-39. doi: 10.5670/oceanog.2011.2

Tsuji, L.J.S., Gomez, N., Mitrovica, J.X., and Kendall, R. (2009). Post-glacial isostatic adjustment and global warming in Subarctic Canada: Implications for islands of the James Bay region. Arctic 62(4):458 – 467. doi: 10.14430/arctic176

Tsuji, L., Daradich, A., Gomez, N., Hay, C., & Mitrovica, J. (2016). Sea Level Change in the Western James Bay Region of Subarctic Ontario: Emergent Land and Implications for Treaty No. 9. Arctic, 69(1), 99. doi: 10.14430/arctic4542

Uehara, K., Scourse, J., Horsburgh, K., Lambeck, K., & Purcell, A. (2006). Tidal evolution of the northwest European shelf seas from the Last Glacial Maximum to the present. *Journal Of Geophysical Research*, *111*(C9). doi: 10.1029/2006jc003531

Weatherall, P., Marks, K., Jakobsson, M., Schmitt, T., Tani, S., & Arndt, J. et al. (2015). A new digital bathymetric model of the world's oceans. *Earth and Space Science*, *2*(8), 331-345. doi: 10.1002/2015ea000107

Webb, D. (2014). On the tides and resonances of Hudson Bay and Hudson Strait. *Ocean Science*, *10*(3), 411-426. doi: 10.5194/os-10-411-2014

Wilmes, S., Green, J., Gomez, N., Rippeth, T., & Lau, H. (2017). Global Tidal Impacts of Large-Scale Ice Sheet Collapses. *Journal of Geophysical Research: Oceans*, *122*(11), 8354-8370. doi: 10.1002/2017jc013109

Winkelmann, R., Martin, M., Haseloff, M., Albrecht, T., Bueler, E., Khroulev, C., & Levermann, A. (2011). The Potsdam Parallel Ice Sheet Model (PISM-PIK) – Part 1: Model description. *The Cryosphere*, *5*(3), 715-726. doi: 10.5194/tc-5-715-2011

Woodward, R. (1888), On the form of and position of mean sea level, *U.S. Geol. Surv. Bull*., 48, 87–170.

WRCP Global Sea Level Budget Group. Global sea-level budget 1993–present. (2018). *Earth System Science Data*, *10*(3), 1551-1590. doi: 10.5194/essd-10-1551-2018

	M_2	S_2	K_1
ETOPO1	70.7 / 36.7 / 38.3	25 / 10.8 / 11.8	4.7 / 3.2 / 4.0
- **HB**	39.2	12.7	3.6
- **HS/FB/CS**	127.8	47.1	6.5
SRTM	50.2 / 33.9 / 37.8	22.2 / 10.3 / 11.6	3.9 / 2.8 / **3.3**
- **HB**	56.6	20.8	4.4
- **HS/FB/CS**	38.5	24.7	2.8
GEBCO 2008	54.3 / 24.2 / 25.3	17.4 / 8.4 / 9.2	3.0 / 3.3 / 4.1
- **HB**	38.3	10.1	3.2
- **HB/FB/CS**	83.3	30.4	2.5
GEBCO 2014	47.8 / 29.8 / 30.9	16.6 / 9.2 / 10.1	3.6 / 2.8 / 3.3
- **HB**	25.8	**5.7**	3.4
- **HB/FB/CS**	87.4	36.0	3.9
COMPOSITE	**19.3 / 14.4 / 15.9**	**11.8 / 4.7 / 5.7**	**2.9** / **2.6** / 3.6
- **HB**	**15.0**	6.6	**3.1**
- **HS/FB/CS**	**27.0**	**21.2**	**2.4**

Table 1: Bathymetry evaluation. Shown are complex elevation errors in cm between the tide model simulations using the respective bathymetry and tide gauges / TPXO8 / TPXO9 for M_2, S_2 and K_1. The best fit has been highlighted for each constituent and evaluation method. For each bathymetry we also show errors against the tide gauges located in Hudson Bay only and the tide gauges located in Hudson Strait (HB), Frobisher Bay (FB) and Cumberland Sound (CS).

Figure 1: Model domain used in this study, showing a) Bathymetry and topography of the Hudson Bay Complex, (data from the composite dataset described in section 3) defined here as Hudson Bay, James Bay, Foxe Basin and Hudson Strait, b) Present day semi-diurnal (M_2) tidal amplitudes (colour) and phases (contoured in white lines at 1/8 M_2 period), taken from the TPXO8 tide database (http://volkov.oce.orst.edu/tides/tpxo8_atlas.html).

Figure 2: Amplitude differences between simulated M_2 amplitudes from several bathymetry datasets and M_2 amplitudes from the TPXO8 tidal solution. a) ETOPO1 (Amante & Eakins, 2009), b) GEBCO 2008 (http://www.gebco.net), c) SRTM30_Plus (Becker et al., 2009), d) GEBCO 2014 (http://www.gebco.net), e) our new, composite bathymetry with SRTM30_Plus in Hudson Bay and GEBCO 2008 elsewhere. The colored circles show the amplitude differences for the tide-gauge locations (see also Text S1 and Table S4).

Figure 3: Contributions to sea level change in the HBC from GIA and future melting of the polar ice sheets under RCP8.5 at 2100, 2300 and 2500, relative to 2000. Blue shading corresponds to a sea level fall and red shading corresponds to a sea level rise. (a-c) Contribution to sea level change from past ice-ocean loading changes (i.e. GIA) over the last deglaciation associated with the ICE-5G ice history (Peltier, 2004). (d-f) Contribution to sea level change from the Greenland Ice Sheet (Golledge et al., 2019). (g-l) Contribution to sea level change from the Antarctic Ice Sheet under from (g-i) low-end (Golledge et al., 2019) and (j-l) high-end (Pollard et al., 2017)

projections. Note the different color scales, the color bar associated with each panel is on the right side of each plot.

Figure 4: Total projected sea level change at 2100, 2300, and 2500, relative to 2000. Sum of individual contributions presented in **Figure 3**. Panels a-c correspond to the low-end Antarctic ice loss scenario (Golledge et al., 2019). Panels d-f correspond to the high-end Antarctic ice loss scenario (Pollard et al., 2017).

Figure 5: Total projected M2 amplitude change at 2100, 2300, and 2500, relative to 2000 for simulations where flooding of low-lying land is permitted with increasing sea levels. Panels a-c correspond to tidal changes associated with the low-end Antarctic ice loss scenario (Golledge et al., 2019). Panels d-f correspond to tidal changes associated with the high-end Antarctic ice loss scenario (Pollard et al., 2017).

Figure 1.

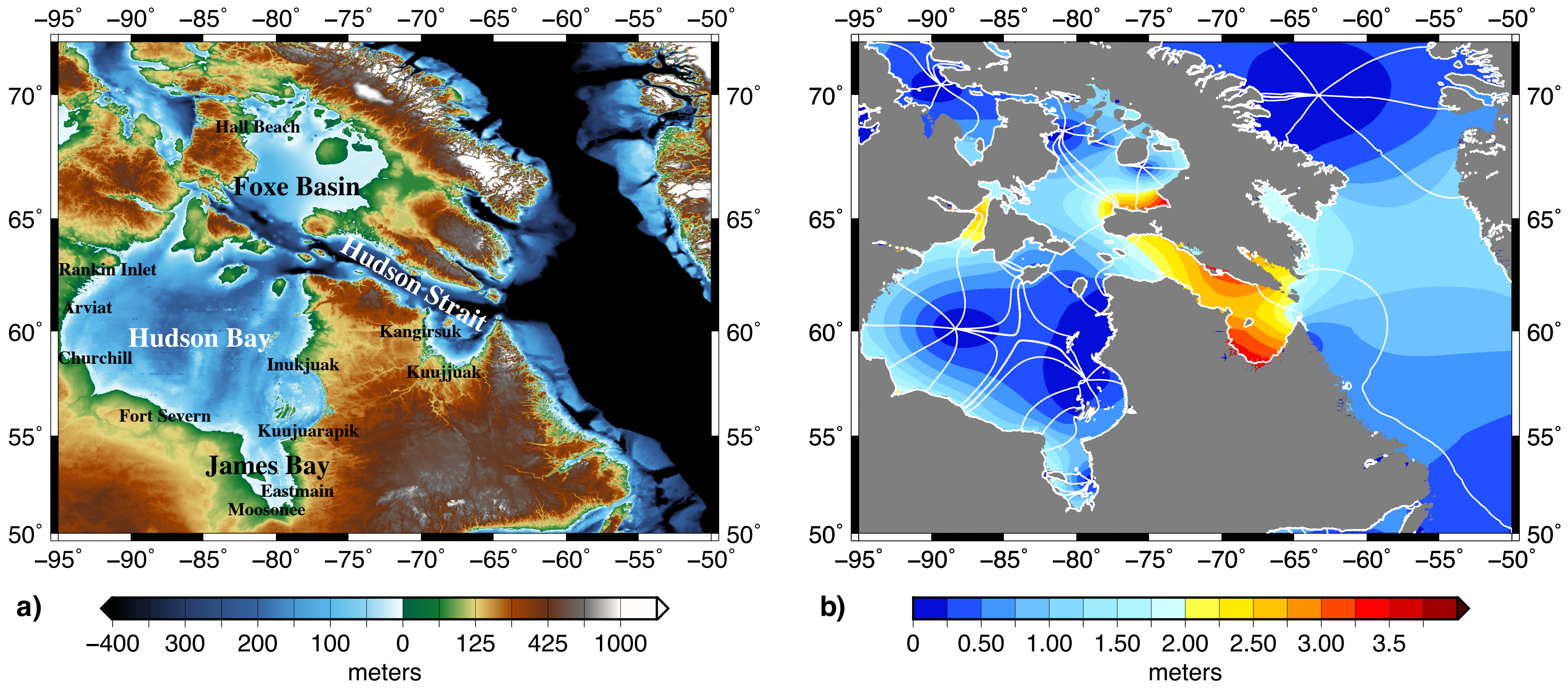

Hall Beach
Foxe Basin
Hudson Strait
Rankin Inlet
Arviat
Hudson Bay
Churchill
Kangirsuk
Inukjuak
Kuujjuak
Fort Severn
Kuujjuarapik
James Bay
Eastmain
Moosonee
a)
−400 300 200 100 0 125 425 1000
meters
b)
0 0.50 1.00 1.50 2.00 2.50 3.00 3.5
meters

Figure 2.

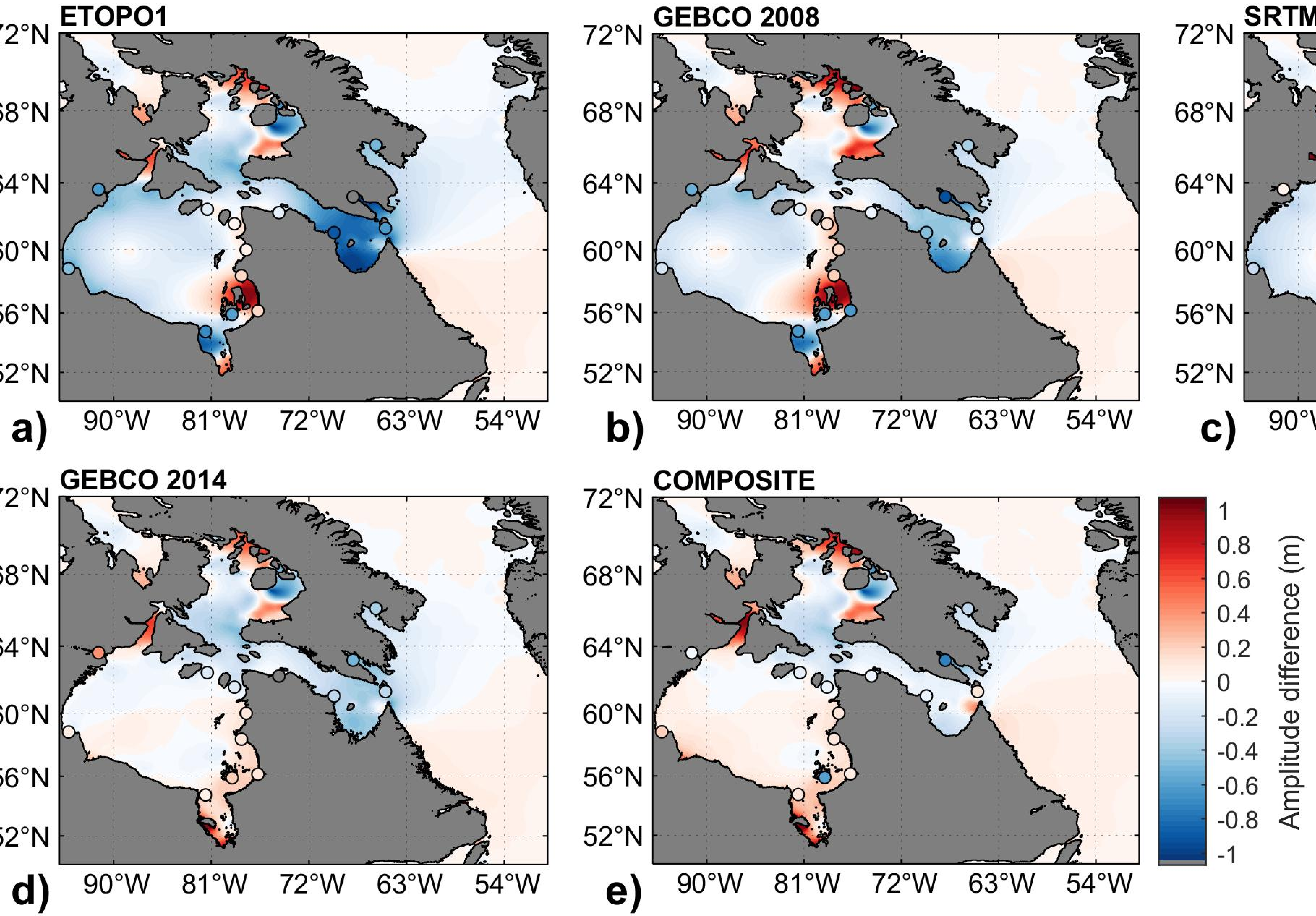
ETOPO1
GEBCO 2008
SRTM
GEBCO 2014
COMPOSITE
72°N
68°N
64°N
60°N
56°N
52°N
90°W
81°W
72°W
63°W
54°W
a)
b)
c)
d)
e)
Amplitude difference (m)
1
0.8
0.6
0.4
0.2
0
-0.2
-0.4
-0.6
-0.8
-1

Figure 3.

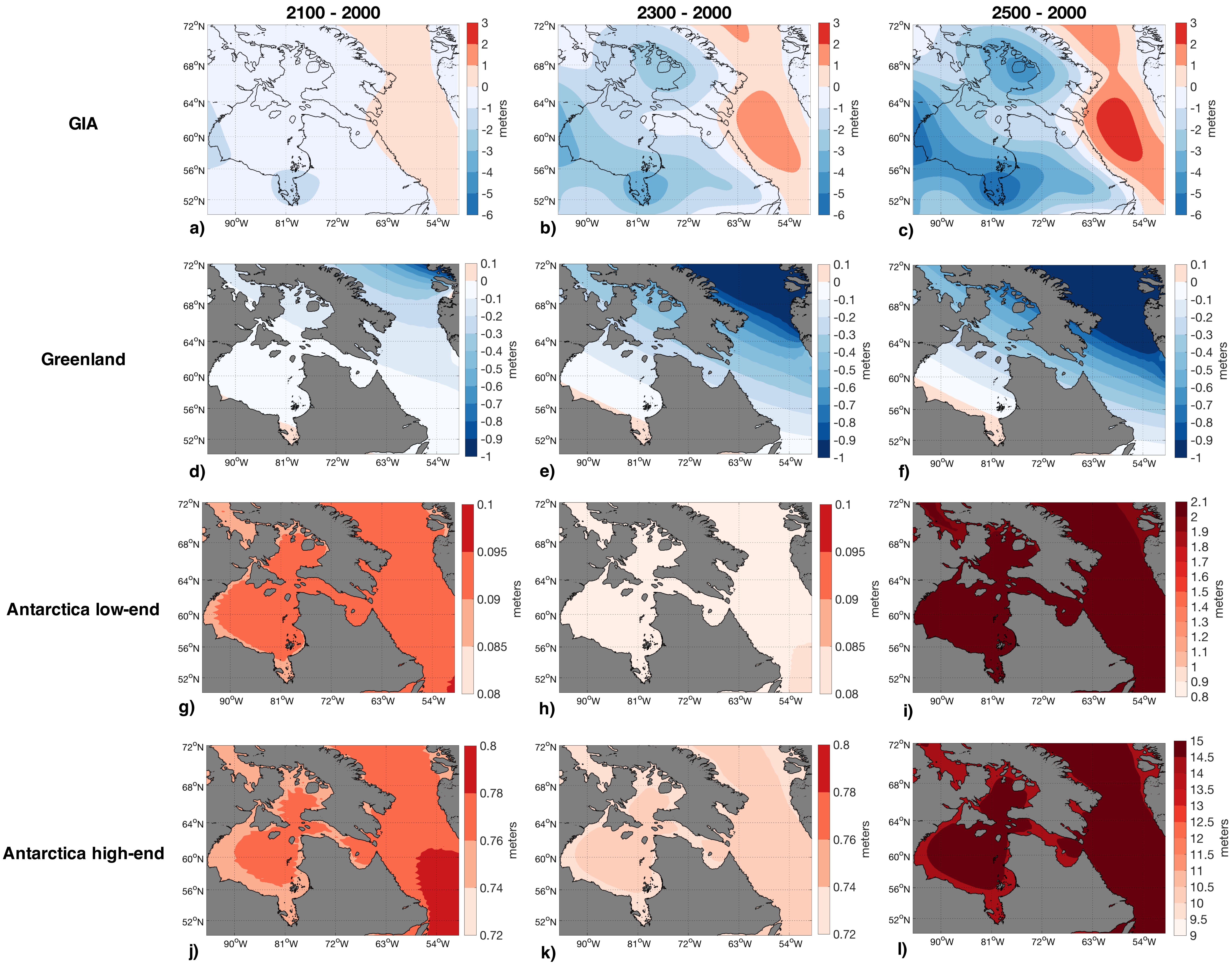

2100 - 2000
2300 - 2000
2500 - 2000
GIA
Greenland
Antarctica low-end
Antarctica high-end
meters
a)
b)
c)
d)
e)
f)
g)
h)
i)
j)
k)
l)

Figure 4.

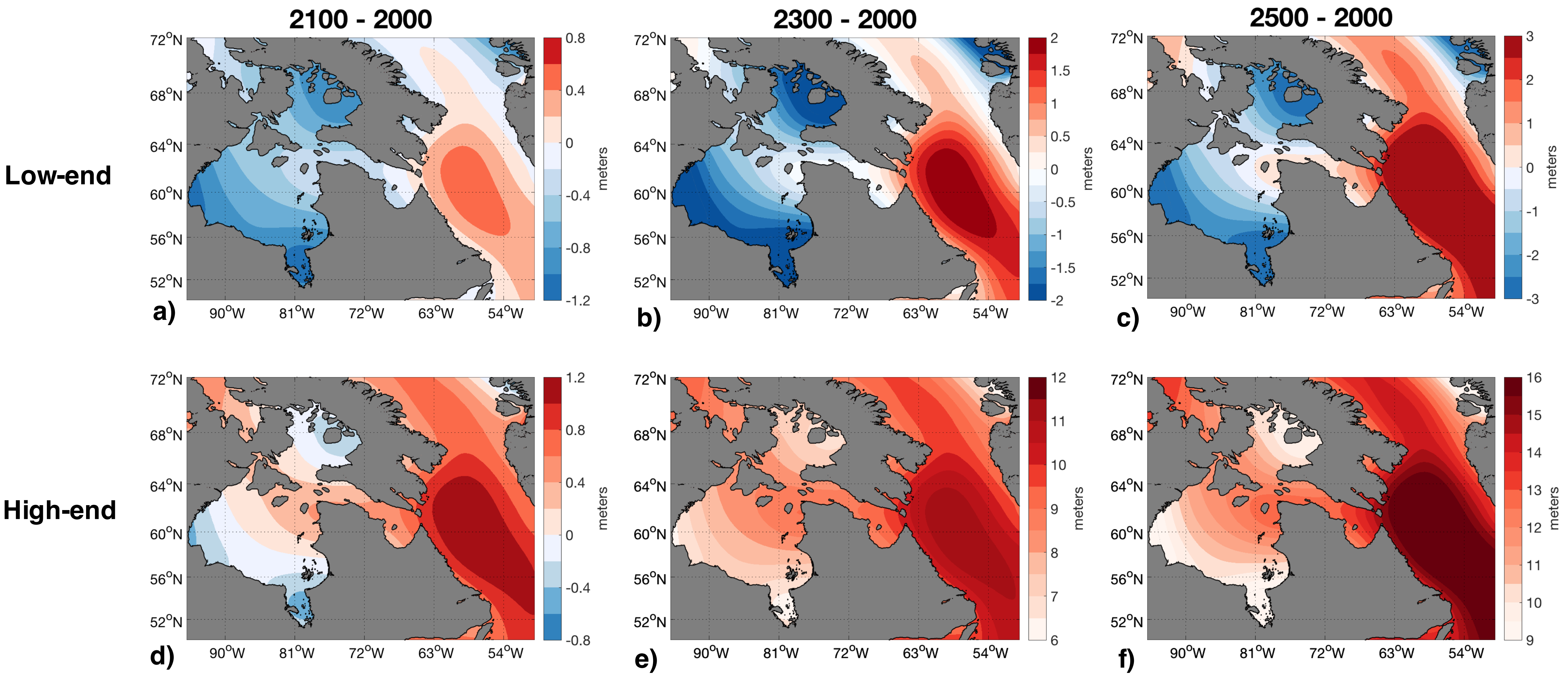
2100 - 2000
2300 - 2000
2500 - 2000
Low-end
High-end
a)
b)
c)
d)
e)
f)
72°N
68°N
64°N
60°N
56°N
52°N
90°W
81°W
72°W
63°W
54°W
meters

Figure 5.

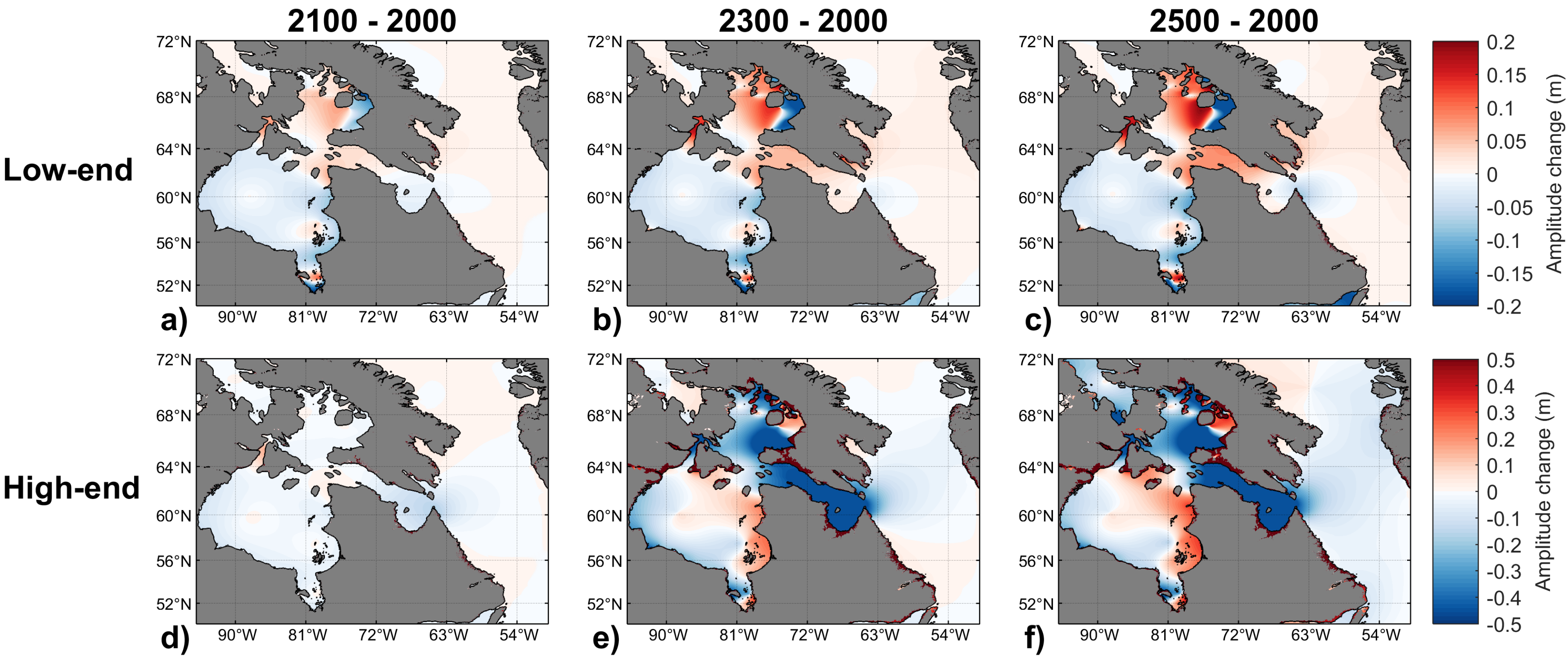
2100 - 2000
2300 - 2000
2500 - 2000
Low-end
High-end
72°N
68°N
64°N
60°N
56°N
52°N
90°W
81°W
72°W
63°W
54°W
a)
b)
c)
d)
e)
f)
0.2
0.15
0.1
0.05
0
-0.05
-0.1
-0.15
-0.2
Amplitude change (m)
0.5
0.4
0.3
0.2
0.1
0
-0.1
-0.2
-0.3
-0.4
-0.5
Amplitude change (m)